World Journal of Gastroenterology

Submit a Manuscript: https://www.f6publishing.com

World J Gastroenterol 2020 March 7; 26(9): 904-917

DOI: 10.3748/wjg.v26.i9.904

ISSN 1007-9327 (print) ISSN 2219-2840 (online)

ORIGINAL ARTICLE

Basic Study

Magnetic resonance imaging biomarkers for pulsed focused ultrasound treatment of pancreatic ductal adenocarcinoma

Ezekiel Maloney, Yak-Nam Wang, Ravneet Vohra, Helena Son, Stella Whang, Tatiana Khokhlova, Joshua Park, Kayla Gravelle, Stephanie Totten, Joo Ha Hwang, Donghoon Lee

ORCID number: Ezekiel Maloney (0000-0002-7614-4399); Yak-Nam Wang (0000-0003-0396-6057); Ravneet Vohra (0000-0001-6258-2710); Helena Son (0000-0003-1776-531X); Stella Whang (0000-0001-5893-6029); Tatiana Khokhlova (0000-0002-1711-0404); Joshua Park (0000-0002-6434-879X); Kayla Gravelle (0000-0002-9724-3134); Stephanie Totten (0000-0002-8848-4745); Joo Ha Hwang (0000-0002-7534-230X); Donghoon Lee (0000-0001-5220-3991).

Author contributions: Maloney E, Wang YN, Vorha R, Son H, Whang S, Khokhlova T, Park J, Gravelle K, and Lee D performed the majority of experiments; Maloney E, Wang YN, Vorha R, and Park J performed the majority of data analysis; Maloney E, Wang YN, and Lee D performed the majority of data interpretation; S Totten assisted Wang YN, S Whang, H Son and K Gravelle in treatment and care of the involved animals, as well as tissue processing/testing; Lee D and Hwang JH designed and coordinated the research; Maloney E wrote the initial draft of the manuscript; Maloney E and Wang YN created the figures; all authors contributed to manuscript content over multiple subsequent rounds of internal editing and revision prior to submission; all authors agreed upon the final content of the manuscript.

Supported by National Institutes of Health, National Cancer Institute, No. R01 CA188654 and No. R01

Ezekiel Maloney, Ravneet Vohra, Joshua Park, Donghoon Lee, Department of Radiology, University of Washington, Seattle, WA 98195, United States

Yak-Nam Wang, Applied Physics Laboratory, University of Washington, Seattle, WA 98195, United States

Helena Son, Stella Whang, Tatiana Khokhlova, Kayla Gravelle, Stephanie Totten, Division of Gastroenterology, University of Washington, Seattle 98195, WA, United States

Joo Ha Hwang, Division of Gastroenterology & Hepatology, Stanford University School of Medicine, Redwood City, CA 94063, United States

Corresponding author: Donghoon Lee, PhD, Research Professor, Department of Radiology, University of Washington, SLU C256, 850 Republican Street, Seattle, WA 98109, United States. dhoonlee@uw.edu

Abstract

BACKGROUND

The robust fibroinflammatory stroma characteristic of pancreatic ductal adenocarcinoma (PDA) impedes effective drug delivery. Pulsed focused ultrasound (pFUS) can disrupt this stroma and has improved survival in an early clinical trial. Non-invasive methods to characterize pFUS treatment effects are desirable for advancement of this promising treatment modality in larger clinical trials.

AIM

To identify promising, non-invasive pre-clinical imaging methods to characterize acute pFUS treatment effects for *in vivo* models of PDA.

METHODS

We utilized quantitative magnetic resonance imaging methods at 14 tesla in three mouse models of PDA (subcutaneous, orthotopic and transgenic - *KrasLSL-G12D/+*, *Trp53LSL-R172H/+*, *Cre* or "KPC") to assess immediate tumor response to pFUS treatment (VIFU 2000 Alpinion Medical Systems; 475 W peak electric power, 1 ms pulse duration, 1 Hz, duty cycle 0.1%) *vs* sham therapy, and correlated our results with histochemical data. These pFUS treatment parameters were previously shown to enhance tumor permeability to chemotherapeutics. T1 and T2 relaxation maps, high (126, 180, 234, 340, 549) *vs* low (7, 47, 81) *b*-value apparent diffusion coefficient (ADC) maps, magnetization transfer ratio (MTR)

CA154451.

Institutional animal care and use committee statement: All animal experiments were conducted in accordance with policies of the NIH Guide for the Care and Use of Laboratory Animals and the Institutional Animal Care and Use Committee (IACUC) of the University of Washington. Specific protocols used in this study were approved by the University of Washington IACUC (approved protocols are: "4210-01: MR Methods for Small Animal Imaging" and "4242-05: Enhanced chemotherapeutic drug delivery by High Intensity Focused Ultrasound").

Conflict-of-interest statement: All other authors have nothing to disclose.

ARRIVE guidelines statement: The authors have read the ARRIVE guidelines, and the manuscript was prepared and revised according to the ARRIVE guidelines.

Manuscript source: Unsolicited manuscript

Received: November 17, 2019
Peer-review started: November 17, 2019
First decision: December 23, 2019
Revised: January 12, 2020
Accepted: February 15, 2020
Article in press: February 15, 2020
Published online: March 7, 2020

P-Reviewer: Huang LY, Mastoraki A
S-Editor: Ma YJ
L-Editor: A
E-Editor: Ma YJ

maps, and chemical exchange saturation transfer (CEST) maps for the amide proton spectrum (3.5 parts per million or "ppm") and the glycosaminoglycan spectrum (0.5-1.5 ppm) were generated and analyzed pre-treatment, and immediately post-treatment, using ImageJ. Animals were sacrificed immediately following post-treatment imaging. The whole-tumor was selected as the region of interest for data analysis and subsequent statistical analysis. *T*-tests and Pearson correlation were used for statistical inference.

RESULTS
Mean high-*b* value ADC measurements increased significantly with pFUS treatment for all models. Mean glycosaminoglycan CEST and T2 measurements decreased significantly post-treatment for the KPC group. Mean MTR and amide CEST values increased significantly for the KPC group. Hyaluronic acid focal intensities in the treated regions were significantly lower following pFUS treatment for all animal models. The magnetic resonance imaging changes observed acutely following pFUS therapy likely reflect: (1) Sequelae of variable degrees of microcapillary hemorrhage (T1, MTR and amide CEST); (2) Lower PDA glycosaminoglycan content and associated water content (glycosaminoglycan CEST, T2 and hyaluronic acid focal intensity); and (3) Improved tumor diffusivity (ADC) post pFUS treatment.

CONCLUSION
T2, glycosaminoglycan CEST, and ADC maps may provide reliable quantitation of acute pFUS treatment effects for patients with PDA.

Key words: Pancreatic adenocarcinoma; Multiparametric magnetic resonance imaging; Focused ultrasound

Core tip: In a genetic model of pancreatic ductal adenocarcinoma, clinically translatable, quantitative magnetic resonance imaging methods of T2, glycosaminoglycan chemical exchange saturation transfer, and apparent diffusion coefficient mapping were effective in non-invasively characterizing the treatment effects of pulsed focused ultrasound treatment. Pulsed focused ultrasound treatment has already been shown to improve survival for patients with pancreatic ductal adenocarcinoma in an early clinical trial, and these complimentary magnetic resonance imaging methods could help to advance this promising therapy in larger clinical trials.

Citation: Maloney E, Wang YN, Vohra R, Son H, Whang S, Khokhlova T, Park J, Gravelle K, Totten S, Hwang JH, Lee D. Magnetic resonance imaging biomarkers for pulsed focused ultrasound treatment of pancreatic ductal adenocarcinoma. *World J Gastroenterol* 2020; 26(9): 904-917
URL: https://www.wjgnet.com/1007-9327/full/v26/i9/904.htm
DOI: https://dx.doi.org/10.3748/wjg.v26.i9.904

INTRODUCTION

Pancreatic cancer is the fourth leading cause of cancer-related deaths in the United States[1]. Pancreatic ductal adenocarcinomas (PDAs) have a robust fibroinflammatory stroma and a dense extracellular matrix that accumulates water molecules in a poorly mobile, gel-fluid phase[2]. In combination, these features result in a high interstitial fluid pressure (IFP; approximately 99 mmHg *vs* 10.4 in normal pancreas) that collapses tumor vasculature and impedes therapeutic drug delivery[2-4]. Glycosaminoglycans produced by PDA tumor cells are often present at exceedingly high concentrations in the tumor interstitium, and their presence correlates with high IFP. In a genetic mouse model of PDA, pulsed focused ultrasound (pFUS) therapy has disrupted the tumor stroma and improved delivery of chemotherapy to the tumor[4,5]. A recent phase 1 clinical trial of pFUS therapy in combination with chemotherapy doubled median overall survival in patients with inoperable PDA *vs* chemotherapy

alone[6]. In clinical trials and in clinical practice, both the time and invasiveness required to assess treatment efficacy are critical considerations for the majority of patients with PDA who have rapidly progressive, non-surgical disease in a highly sensitive anatomic area. Quantitative magnetic resonance imaging (MRI) assessments at 14 tesla (T) have previously been shown to correlate well with the degree of PDA fibrosis in preclinical models[7]. In this study, our objective was to identify non-invasive MRI methods that can be used to assess pFUS treatment effects for PDA, based on data derived from three murine models of PDA, including a genetic model. These methods have translational relevance to future, larger clinical trials that might help to advance pFUS therapy as a valuable supplement to traditional treatment modalities for patients with PDA.

MATERIALS AND METHODS

Animal models

All animal studies were approved by the Institutional Animal Care and Use Committee of the University of Washington. The animal protocol was designed to minimize pain or discomfort to the animals included in our study. Subcutaneous, orthotopic, and genetic murine models of PDA were employed. We used the *KrasLSL-G12D/+*, *Trp53LSL-R172H/+*, *Cre* (KPC) genetic PDA mouse model[8]. KPC animals conditionally express endogenous mutant *Kras* and point mutant *Trp53* alleles, spontaneously develop PDA, and closely mimic the pathophysiology and molecular progression of the human disease[8]. All mice were housed in an specific pathogen free, controlled environment (14 h/10 h light/dark cycle, 73.5 ± 5 °F) with ad libitum access to tap water and chow. We used previously described methods to develop orthotopic models[7,9]. Briefly, 8-10 wk old, immunocompetent mixed *129/SvJae/C57Bl/6* mice were anesthetized and, following sterile preparation, a 2 cm incision was made along the left flank to access the tail of the pancreas. One million cells derived from KPC liver metastases, suspended in 50 microliters of Matrigel (Corning Incorporated), were injected into the pancreatic tail. The incision was sutured closed and the animal was recovered. For subcutaneous models, the same cell suspension was injected at the left flank, near the hindlimb. At 12-14 wk old, all animal models underwent weekly tumor burden monitoring with direct palpation and diagnostic ultrasound (US). Animals were enrolled in the study when their primary tumor mass was ≥ 5 mm in greatest diameter. Six KPC animals, 6 orthotopic model animals, and 6 subcutaneous model animals were enrolled and underwent the MRI and pFUS treatment protocols. Between 3 and 5 additional animals for each tumor model underwent the same MRI protocol, but with sham treatment. The size of each experimental group was previously approved by the National Institutes of Health funding agency, based on result from prior similarly designed studies, to ensure reasonable ability to detect any meaningful data trends in this early phase research.

MRI protocol

Our group has previously used quantitative MRI methods at 14T magnet strength to characterize both untreated PDA tumors in subcutaneous, orthotopic, and KPC models, as well as enzymatically treated PDA tumors in KPC models[7,10]. Similar quantitative methods were employed in the current study for in-vivo assessments on a 14T Avance 600 MHz/89 mm wide-bore vertical MR spectrometer with a microimaging accessory (Bruker BioSpin corp., Bellerica, MA, United States) using a ^{1}H radiofrequency birdcage coil and coil holder with 25 mm inner diameter. Quantitative MRI parameter acquisition methods are detailed in Table 1. The water saturation shift referencing approach to chemical exchange saturation transfer (CEST) imaging has also been used by other laboratories at 3-9.4 T magnet strength for pre-clinical applications, including murine tumor model imaging, with reliable quantitative results[11-13].

As previously described, animals were anesthetized, lubricant was applied to their eyes, they were placed into a radiofrequency coil and secure custom cradle that was inserted vertically into the thermally-regulated (32 °C) magnet bore[7]. An adjustable isoflurane gas/vacuum system was used to maintain appropriate sedation throughout the experiments. The animals' respiratory rates were monitored continuously for the approximately 60 min scan time via abdominal sensor (SA Instruments Inc., Stony Brook, NY). A baseline MRI assessment was performed for each animal within 1.5 wk of enrollment and 48 h prior to pFUS or sham therapy. Immediately post-therapy, animals underwent a follow-up MRI assessment. Animals were sacrificed for histochemical analysis after being removed from the scanner at the conclusion of the follow-up MRI.

Table 1 14T magnetic resonance imaging parameter acquisition methods

Method	Sequence type	TR/TE (ms)	Comments
T1	RARE	5500, 3000, 1500, 1000, 385.8/9.66	NA = 1; FOV = 30 mm × 30 mm; rare factor = 2, matrix size = 256 × 128 (reconstructed phase encoding steps = 128; acquisition phase encoding steps = 96); yielding spatial resolution of 0.117 × 0.234 mm/pixel. Approximately 9 min acquisition time.
T2	MSME, fat suppressed	4000/twelve echoes equally spaced from 6.28 to 75.4	NA = 1; FOV = 30 mm × 30 mm; matrix size = 256 × 128 (reconstructed phase encoding steps = 128; acquisition phase encoding steps = 91); spatial resolution of 0.117 × 0.234 mm/pixel. 10 contiguous slices were acquired with respiration gating to cover the entire abdomen. Approximately 6 min acquisition time.
ADC	EPI	2500/17.7	Echo train length = 16; Pulse duration = 3.0 ms; Diffusion time = 7.46 ms; NA = 1; FOV = 30 × 30 mm^2; matrix size = 128 × 128; spatial resolution of 0.234 × 0.234 mm/pixel; 8 *b* values (7, 47, 81, 126, 180, 234, 340, 549) s/mm^2. 10 contiguous slices were acquired to cover the entire abdomen. Approximately 2 min 40 s acquisition time.
CEST	(1) RARE	(1) 2200 / 7	(1) Center frequency estimate: Continuous-wave block saturation pulse with B1 = 3 μT and duration = 1 s; 25 frequency offsets from -360 Hz to 360 Hz with an interval of 0.5 ppm (WASSR approach). FOV = 30 mm x 30 mm; Matrix size = 128 x 128; Flip angle = 180°; NA = 1. A single, 1 mm slice delineating the tumor was acquired.
	(2) RARE	(2) 5000 / 7	(2) Frequency shift saturation: 14 frequency offsets at ± 0.5, ± 1.0. ± 1.5, ± 2.0, ± 2.5, ± 3.0, ± 3.5 ppm were acquired through the same single slice using respiration gating with an off-resonance radiofrequency pulse applied for 1 s at a power of 3 μT. Matrix = 128 × 128 (reconstructed phase encoding steps = 128; acquisition phase encoding steps = 96); FOV = 30 mm × 30 mm; rare factor = 8.
	(3) RARE	(3) 5000 / 7	(3) Control image: A control image was acquired through the same slice using the same settings as #2, except with saturation offset at 300 ppm. Approximately 30 min total acquisition time.
MTR	GRE	625 / 2	Flip angle = 30°; off-resonance frequency 7000 Hz; saturation pulse block pulse shape = 50 ms width and 10 μT amplitude; FOV = 30 mm × 30 mm; matrix size = 256 × 256; spatial resolution of 0.117 x 0.117 mm/pixel. 10 contiguous images were acquired to cover the entire abdomen. Approximately 3 min acquisition time.

ADC: Apparent diffusion coefficient; CEST: Chemical exchange saturation transfer; MTR: Magnetization transfer ratio.

MRI quantitative map creation and data analysis

Raw MR images were processed for map creation using Image-J software (Rasband, W.S., ImageJ, United States National Institutes of Health, Bethesda, ML, http://imagej.nih.gov/ij, 1997-2012)[14]. T1 and T2 relaxation maps were generated from T1 and T2 weighted images. Apparent diffusion coefficient (ADC) maps were generated using a mono-exponential model: Sb/S0 = exp(-b·ADC). Sb represents the MRI signal intensity with diffusion weighting b and S0 represents the non-diffusion-weighted signal intensity. A bi-exponential model was also used to estimate intra voxel incoherent motion (IVIM) related parameters of perfusion fraction (or pseudo-diffusion) and diffusion[15]. The 3 lowest b values (7, 47, and 81 s/mm^2) were used to calculate perfusion / pseudo-diffusion component, and the remaining higher 5 *b* values (126, 180, 234, 340, 549 s/mm^2) were used to calculate the tissue diffusivity parameter. Magnetization transfer ratio (MTR) maps were generated using: (SI0–SIs)/SI0, where SI0 represents the tissue signal intensity prior to application of the saturation pulse, and SIs represents the tissue signal intensity during the saturation pulse application. CEST maps were generated for the amide proton using: [Ssat (-3.5 ppm) - Ssat (3.5 ppm)]/S0, where S0 and Ssat are the water signal intensities measured prior to the saturation pulse, and during the water saturation pulse, respectively. For the glycosaminoglycan spectrum (gagCEST), maps were generated using a similar calculation for the 0.5, 1.0 and 1.5 ppm frequency shifts. Summative saturation sampled at these shifts has previously been validated in human cartilage for quantification of glycosaminoglycans[16], and is representative of the spectral signal observed in prior 7T MRI studies of glycosaminoglycan phantoms[17], as well as our own phantom studies at 14T[10]. Ultimately, CEST measurements were not performed in the subcutaneous mice due to the difficulty in properly performing the shimming process for these animals. A susceptibility change near the interface between a subcutaneous tumor and air often precluded adequate shimming and tumor signal suppression.

pFUS treatment protocol and cavitation quantitation

Animals were anesthetized and the abdomen was shaved, depilated, and wiped with isopropyl alcohol to decrease risk of cavitation at the skin surface. Animals were then mounted to a custom holder capable of 3 dimensional movement for positioning during treatment, and partially submerged in a 37 °C, transparent water tank, where respiratory rate could be constantly visually monitored during continuous anesthesia throughout the experiment. pFUS treatments were performed under US guidance with an Alpinion VIFU 2000 small animal system. A 1.5 MHz focused US transducer with a 64 mm aperture and 45 mm radius of curvature was mounted to the side of the water tank[18]. A miniature flat passive cavitation detector (Panametrics XMS-310; Olympus, Waltham, Mass) was positioned at the side of the transducer and aligned to detect broadband emissions from inertially collapsing bubbles in the focal area during each FUS pulse. The passive cavitation detector was 3 mm in aperture, with the frequency band of 6.3-14.2 MHz at a 6-dB level. The signals received by the passive cavitation detector were amplified by 20 dB (Panametrics PR5072; Olympus) and recorded by using a digital oscilloscope[19]. The US imaging probe employed a C4-12 phased array, with center frequency 7 MHz (Alpinion Medical Systems). The tumor was identified as a predominantly hypoechoic mass, typically in the epigastrium or along the left paracolic gutter adjacent to the spleen. Assessment was made for an appropriate acoustic treatment window that was free of intervening loops of bowel or significant vasculature. For the KPC animal cohort, whose tumors were less commonly superficial, the presence of an appropriate treatment window always determined whether the animal would receive pFUS *vs* sham treatment. For the orthotopic and subcutaneous model cohorts, receipt of sham *vs* pFUS treatment was randomized.

Exposure parameters were: Peak electric power 475 watts, pulse duration 1 ms, pulse repetition frequency 1 Hz, duty cycle 0.1%. The focal spot was raster-scanned throughout the acoustically accessible volume of the tumor with a step size of 1 mm, and 60 pulses were delivered at each focal spot. These parameters were previously shown to enhance tumor permeability to chemotherapeutics[4]. Cavitation activity was quantitated based on broadband noise emission as previously described[18]. Sham treatment animals remained submerged in the water tank under anesthesia for the same duration of time required to deliver the pFUS therapy, but did not receive the therapy. At the completion of the pFUS or sham treatment session (approximately 20 min duration), while maintaining anesthesia, animals were removed from the water tank, dried, and placed on a warming pad for transport to the adjacent MRI suite and follow-up imaging. At the end of the study, the animals were immediately euthanized according to approved procedures for the collection of biological samples.

Histology and biochemistry

Tumors were excised and embedded in an optimum cutting temperature medium. Three serial 5 micrometer sections were cut every 1 mm through the entire tumor (CM1950, Leica, Bannockburn, IL, United States). Tissue between the section steps was collected for biochemical analysis. Samples taken for biochemical analysis were evaluated for sulfated glycosaminoglycans (sGAG) and hyaluronan (HA) using commercial assays (Blyscan™ for sGAG and Purple-Jelley for HA, Biocolor Ltd., United Kingdom).

Tissue sections were stained with Hematoxylin and Eosin (H&E), Masson's trichrome for connective tissue and for HA using a HA binding protein (HABP, Millipore Sigma, Burlington, MA, United States). Sections were examined using a Nikon Eclipse 80i light microscope (Nikon, Melville, NY, United States) and whole slide images were captured for image analysis with a 10 × objective lens using the same settings for each type of stain. Fibrotic tissue, identified by blue staining in the Masson's trichrome stained sections was quantified using methods described previously. For quantification of the HABP stained sections, a random grid of circular regions of interest (ROIs) were placed on each slide. Two random numbers were generated with the first number designating the offset ROI and the second number indicating the sampling number for the ROI selection resulting in several ROIs being evaluated per section. New random numbers were generated for each section. For each ROI selected, the mean intensity was measured ImageJ (ImageJ 1.42 National Institutes of Health, Bethesda, MD, United States). Data was separated into three groups: background (no tissue), non-treated tumor tissue, and FUS treated tissue. FUS treated tissue was identified and confirmed by looking at H&E stained serial sections.

Statistical analysis

For all quantitative maps, the whole tumor that was visible on each analyzed slice was selected as the ROI, and mean quantitative values were recorded for each slice analyzed. On T1, T2, MTR, and ADC maps, this involved selection of 3 separate slices that included the tumor, and the area of the tumor that was ultimately treated for animals who underwent pFUS therapy, on both baseline and follow up MRI exams. The average of the 3 values generated from these slices was used as the single parameter value for the corresponding animal at each point in time. Since CEST maps were only generated for a single slice through the tumor, only 1 whole tumor ROI was used to estimate this parameter at each point in time for the primary analysis comparing pre and post-treatment maps. A secondary analysis of the gagCEST maps using only the follow-up MRI examination maps was performed for the KPC cohort. This secondary analysis method also closely mirrored our histochemical analysis, which was limited to the follow-up time point. In the secondary MRI analysis, an ROI was drawn to select the treated region of the tumor, and a second ROI was drawn to select an untreated region for comparison. For the histological samples, the mean intensities from the treated and untreated ROIs of each tumor were calculated for comparison.

Paired *t*-tests were performed using Microsoft Excel software (Redmond, WA, United States) to compare baseline and follow-up whole-tumor ROI quantitations and to compare treated-tumor *vs* untreated-tumor ROIs. Unpaired t-tests were performed to compare treated and sham treated mice. Statistical significance was assigned to P values less than 0.05. To compare gagCEST values obtained from CEST maps to sGAG values obtained from biochemical analysis, the correlation coefficient (r) was determined using Pearson correlation analysis using StatPlus software (AnalystSoft Inc. Walnut, CA, United States) in Microsoft Excel. Statistical review of the study was performed by a biomedical statistician employed at the University of Washington.

RESULTS

At enrollment into the study the animals had a good body condition score with an average age (± SD) and weight (± SD) of 179 ± 35 d and 26.3 ± 2.8 g respectively. Cavitation activity was achieved in all three murine PDA models and all acquired data from all animals in each group were included in the analysis, with the exception of erroneous amide CEST data from 2 pFUS treated KPC animals and all CEST data from 1 pFUS treated orthotopic animal. No adverse events, such as skin burns or unexpected morbidity/mortality, were observed. Quantitative MRI map analysis results from the pFUS treated animal cohorts are presented in Table 2. Following pFUS treatment (Figure 1), mean high-*b* value ADC values increased significantly for all animal models, and this increase was most pronounced in the KPC model (Figure 2A and B). Mean gagCEST and T2 values decreased significantly post-treatment only

for the KPC group (Figure 2C and D). Mean MTR and amide CEST values increased significantly for the KPC group. Treated areas demonstrated predominantly isointense signal on proton density weighted images, in some instances with an associated peripheral ring of hypointense signal (Figure 1C and F). Overall, there was no significant difference in mean tumor T1 relaxation time values. Parameters tested were otherwise not significantly changed post-pFUS treatment in all three murine PDA models. There were no significant differences in any parameters tested for the sham group animals. There was greater variability within these paired data groups, likely related to their smaller group size, but on review of individual parameter data obtained from each sham animal, no consistent trends were evident between the two timepoints.

There was no statistical difference in HA or sGAG concentration between KPC or orthotopic mice. HA and sGAG mean tissue concentrations were found to be lower in all of the pFUS-treated animals *vs* sham-treatment controls, but these differences were not statistically significant (Figure 3A). The evaluation of the regional concentrations of HA using HABP, showed that the treated regions had significantly lower mean HA labelling intensity in the treated regions compared to the non-treated regions for all animal models (Figure 3B and C). The HA intensities were similar for the KPC and orthotopic mice and lower for the subcutaneous mice (Figure 3B). There was no statistical difference in the mean collagen concentration in the treated region vs the non-treated regions or the sham treated mice.

There was a strong positive correlation between the HA concentrations (as determined by the biochemical assay) and the gagCEST measurements (Figure 4) for the orthotopic (correlation coefficients: 0.72 treated; 0.74 sham) and KPC mice (correlation coefficient: 0.60 treated). There were not enough values to evaluate any correlation for the sham treated KPC mice.

DISCUSSION

T1, MTR and amide CEST

Variable changes in T1 relaxation, and significantly increased MTR and amide CEST signals post-pFUS-treatment most likely represent sequelae of hyperacute hemorrhage from microcapillary vessels. T1 weighted images combined with susceptibility weighted images (SWI) are standard of care for hemorrhage detection and characterization. At the hyperacute time point, T1 weighted images of hemorrhage are typically isointense, and thus would contribute a variable amount of signal to the values generated, as we observed. Amide proton imaging has recently been shown to be even more sensitive and specific for detection and characterization of intracranial hemorrhage than SWI, including at the hyperacute timepoint[20]. Since the broad spectrum of the MTR asymmetry signal includes the region of the amide proton at 3.5 ppm, the increased values from both of these maps would not be surprising in the context of acute hemorrhage.

There are additional factors that also might contribute, in part, to these signal changes. Tumor metabolites such as glucose (3.83 ppm), taurine (3.27 ppm) and ethanolamine (3.13 ppm) are known to be upregulated in PDA, and these could potentially also contribute signal near the amide proton 3.5 ppm frequency shift[21]. However, given the short amount of time that elapsed between pFUS treatment and post-treatment MRI characterization (approximately 15 min), a significant change in the concentration of these metabolites is unlikely. MTR values have also previously been shown to have a positive correlation with the degree of fibrosis in murine PDA tumor models[7,22]. Since the pFUS protocol we employed for our treatments is known to disrupt the collagenous tumor stroma[4], as was observed on Masson's trichrome stains in our study, the signal increase observed on MTR maps post-pFUS is unlikely to be representative of this change. Rather, the signal likely derived from microcapillary hemorrhage at the amide proton portion of the MTR spectrum appears to have dominated MTR values at this time point.

gagCEST, T2 and ADC

Significant decreases in gagCEST and T2 relaxation may represent disruption of glycosaminoglycans within the tumor stroma and associated liberation of complexed water molecules from the gel-fluid phase. This, in combination with disruption of the collagenous matrix, could lead to decreased intra-tumoral IFP and increased diffusivity within the tumor microenvironment[2]. This theory is supported by our quantitative immunohistochemistry results – demonstrating a trend of lower HA and sGAG concentrations on average in pFUS-treated animals *vs* sham treated controls. Although multiple species of sulfated (*e.g.*, chondroitin sulfate) and unsulfated (*e.g.*,

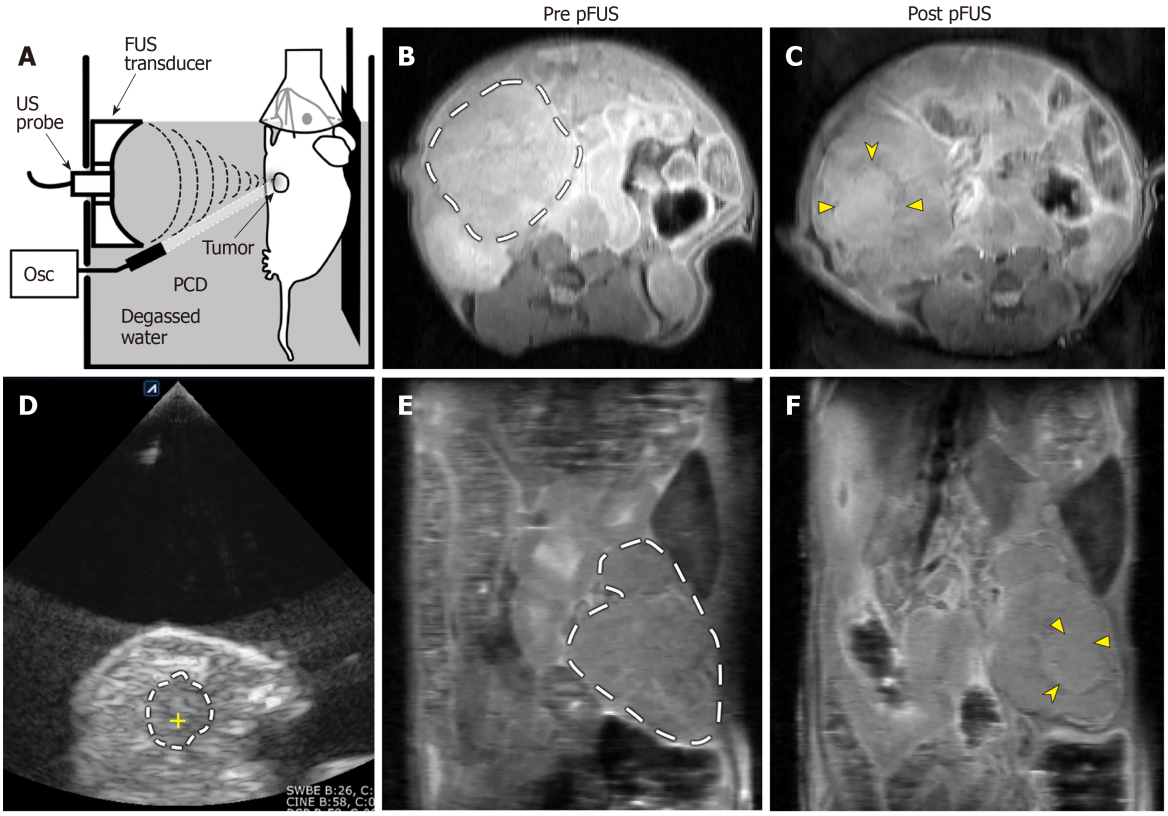

Figure 1 Representative images of pulsed focused ultrasound treatment and 14T magnetic resonance imaging assessment. (A) Sagittal plane line drawing and (D) axial plane ultrasound (US) image of a pulsed focused ultrasound (pFUS) treatment. Animals were anesthetized, placed on a mobile platform, and partially submerged in degassed water. Tumors were identified using B-mode images from a diagnostic US probe. The KPC mouse tumors generally appear as predominantly hypoechoic masses along the distribution of the pancreas (dashed line in D; the yellow cross within marks the focus of the pFUS transducer). Axial (B and C) and coronal (E and F) pre- and post-treatment proton density weighted anatomic images from a different KPC mouse. Dashed lines in B and E demarcate the pancreatic tumor mass. The treated area demonstrates predominantly isointense signal (solid arrowheads in C and F), with a peripheral ring of hypointense signal (notched arrowheads in C and F), most likely representing sequelae of hyperacute hemorrhage. pFUS: Pulsed focused ultrasound; SC: Subcutaneous; Osc: Oscilloscope; PCD: Passive cavitation detector.

HA) glycosasminoglycans are commonly overexpressed in the PDA microenvironment, the HA subtype exerts the dominant effect on IFP[2,23]. Previous phantom imaging experiments by our group, employing a range of relevant concentrations of both chondroitin sulfate and HA, have demonstrated that HA produces a significantly stronger signal on gagCEST imaging at 14T compared to CS, even at 10 fold lower concentrations (*e.g.*, an area under the MTR asymmetry curve of 7.5 for a 0.01% aqueous HA resuspension, *vs* 1.6 for a 0.1% aqueous chondroitin sulfate resuspension)[10]. In addition, we have previously shown that targeted depletion of HA via a systemic enzymatic therapy results in decreased gagCEST signal in KPC mice[10]. These findings support the theory that the signal changes observed post-pFUS treatment on the gagCEST sequence are driven by changes induced in HA concentrations.

There are other, less likely considerations that might explain, or at least contribute to the observed changes in gagCEST signal. Nuclear Overhause Effects (NOE) can spuriously contribute to CEST signal at any portion of the spectrum, and are known to be more prevalent at higher magnet strengths, however we employed high saturation power (3.0 μT) to minimize this potential confounding influence on the signal we obtained.

PDA typically demonstrates restricted diffusion (at or below an arbitrary, sometimes clinically used ADC threshold of 1×10^{-3} mm^2/s), and this is most consistently demonstrated clinically with b values between 500 and 1000[24]. The degree of restriction has been inconsistently correlated with fibrotic content, histopathologic grade, and tumor stage[24]. The degree of restriction may correlate with greater HA content in PDA tumors, given the known positive correlation between HA content and IFP in these tumors[2]. We did not detect such a correlation between whole-tumor HA content and ADC values in the animals we studied. However, there was small variability in the whole-tumor HA content of the animals included in our study, and this limited our ability to detect such a correlation. The limited variability

Table 2 Magnetic resonance imaging quantitative map results pre and post focused ultrasound treatment for three mouse models of pancreatic ductal adenocarcinoma

	Pre-pFUS	Post-pFUS	Difference	*P* value
High-b ADC (10^{-3} mm^2/s)				
KPC	1.0 ± 0.33 (n = 6)	3.32 ± 0.61 (n = 6)	2.32 ± 0.60	**0.01**
Ortho	0.72 ± 0.07 (n = 6)	1.15 ± 0.15 (n = 6)	0.43 ± 0.13	**0.02**
SC	0.97 ± 0.21 (n = 6)	1.80 ± 0.14 (n = 6)	0.83 ± 0.27	**0.03**
GagCEST (%)				
KPC[1]	25.89 ± 3.10 (n = 6)	10.61 ± 3.09 (n = 6)	-15.28 ± 2.67	**2.2×10^{-3}**
Ortho	20.83 ± 4.02 (n = 5)	20.04 ± 5.34 (n = 5)	-0.79 ± 6.41	0.91
Amide CEST (%)				
KPC	10.37 ± 2.76 (n = 4)	24.89 ± 5.17 (n = 4)	14.52 ± 2.89	**0.01**
Ortho	4.11 ± 1.25(n = 5)	4.79 ± 1.64 (n = 5)	0.68 ± 1.99	0.29
MTR (%)				
KPC	38.15 ± 4.17 (n = 6)	59.80 ± 1.46 (n = 6)	21.65 ± 2.96	**7.5×10^{-4}**
Ortho	53.92 ± 7.20 (n = 6)	60.91 ± 3.39 (n = 6)	6.99 ± 6.33	0.32
SC	58.1 ± 7.01 (n = 6)	60.50 ± 7.85 (n = 6)	2.40 ± 7.22	0.75
T2 (ms)				
KPC	39.38 ± 2.32 (n = 6)	34.41 ± 1.93 (n = 6)	-4.97 ± 1.37	**0.02**
Ortho	32.74 ± 1.12 (n = 6)	31.91 ± 0.89 (n = 6)	-0.83 ± 1.54	0.62
SC	44.52 ± 8.97 (n = 6)	32.77 ± 1.67 (n = 6)	-11.75 ± 10.08	0.30
T1 (ms)				
KPC	986.95 ± 236.99 (n = 6)	847.69 ± 255.94 (n = 6)	-139.26 ± 314.92	0.68
Ortho	453.62 ± 116.72 (n = 6)	618.10 ± 183.85 (n = 6)	164.48 ± 194.29	0.44
SC	508.82 ± 192.64 (n = 6)	1032.44 ± 293.46 (n = 6)	523.62 ± 255.40	0.10

Pre and post treatment quantitative values are presented as mean ± SE from the mean. Paired t-tests were used to generate P-values, and values < 0.05, considered significant, are in bold.

[1]Post-hoc secondary analysis, performed to compare the pre and post-treatment KPC groups with gagCEST maps, that employed within-tumor regions of interest (ROIs) rather than whole tumor ROIs, as detailed in the text, generated mean gagCEST values (%) of 25.20 ± 4.63 pre-treatment *vs* 7.71 ± 2.22 post-treatment, for a difference of -17.49 ± 3.07, $P = 6.7 \times 10^{-3}$. pFUS: Pulsed focused ultrasound treatment; ADC: Apparent diffusion coefficient; KPC: Genetic mouse model; Ortho: Orthotopic; SC: Subcutaneous; gagCEST: Glycosaminoglycan chemical exchange saturation transfer; MTR: Magnetization transfer ratio.

in whole-tumor HA content in our animal cohort is likely explained by two factors: (1) We recruited animals into the study when their tumors reached a similar size, and tumor HA content has been shown in a recent clinical series to correlate with tumor size[25]; and (2) For animals undergoing pFUS treatment, the area of treatment, as judged by changes evident on whole-tumor immunohistochemistry slides, involved less than approximately 20% of the overall tumor volume.

It is interesting that a statistically significant decrease in gagCEST and T2 values was only observed in the KPC animal cohort. The gagCEST values correlated well with the total HA concentration in the treated KPC mice and both the treated and sham treated orthotopic mice. When looking at the localized concentrations of HA in the treated tumors, there was a significant decrease in HA in the treated area compared to the surrounding non-treated area. The decrease in HA could potentially result in a decrease in IFP in these regions given the positive correlation between the two[2]. However, this would need to be confirmed experimentally.

Limitations

Limitations of this study include the fact that the whole tumor was selected as the ROI for the primary a priori MR analysis plan. In the treated animals this combined the signal coming from the treated and non-treated regions of the tumor, and decreased our sensitivity for detecting significant treatment effects on tumor signal. This approach was chosen due to the difficulty in determining the precise treatment effect margins on MRI for every tumor treated on any given sequence, which we had encountered in prior experiments with this tumor model. While the general area of treatment could in all cases be identified by correlation between US treatment images and variable changes on T1 and T2 anatomic imaging during MRI scanning, treatment signal effect margins were often ill-defined. Non-standardized, potentially error prone ROI selection in the area of treatment signal changes would have introduced

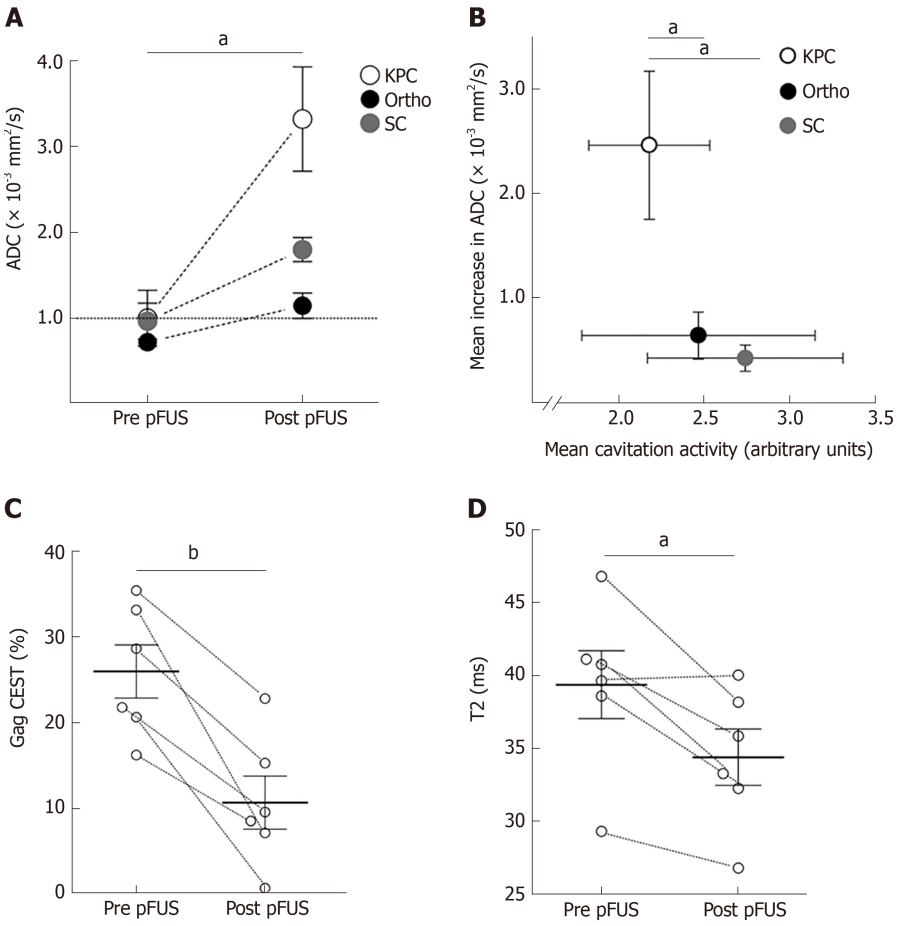

Figure 2 14T magnetic resonance imaging parameter changes due to pulsed focused ultrasound treatments. A: There was significant increase in mean apparent diffusion coefficient (ADC) quantitation for all three murine pancreatic ductal adenocarcinoma models (n = 6 in each group). The horizontal dotted line at ADC = 1 demarcates a frequently used clinical threshold for "restricted" diffusion; B: Cavitation was successfully achieved in all treated animals. On average, cavitation activity tended to be lower in the KPC animals, yet the absolute increase in ADC values for these animals was significantly higher than the other two models post-pulsed focused ultrasound (pFUS) treatment; C and D: GagCEST (C) and T2 (D) quantifications in KPC animals revealed significant decrease in mean values (solid horizontal lines) post-pFUS treatment (n = 6). There was no significant change in these parameters in the other tumor models. [a]P < 0.05; [b]P < 0.01. ADC: Apparent diffusion coefficient; pFUS: Pulsed focused ultrasound; Ortho: Orthotopic; KPC: Genetic mouse model; SC: Subcutaneous.

too great a risk of excluding meaningful data and including irrelevant data in the primary analysis for our relatively small cohort. Whole tumor ROI selection allowed for standard, reliable methodology across all tumor models. Nonetheless, we chose to perform one post-hoc secondary analysis attempting within-tumor ROI selections for the gagCEST sequence in the KPC animals. This was done to compare background tumor *vs* the treated area at a single time point immediately post treatment, to most closely mimic our histologic within-tumor gag quantitative methods. The result of this secondary analysis was consistent with the whole-tumor ROI analysis that compared data from two separate time-points (pre-treatment *vs* immediately post-treatment) – both demonstrated a significant reduction in gagCEST post pFUS treatment.

Subject motion and bowel peristalsis / motion within the abdomen are also inherent limitations of abdominal MRI examinations, and are particularly challenging in small animal models such as ours. Although we attempted to mitigate this effect by continuously monitoring subject respiratory rate throughout image acquisition and use of respiratory gating within sequence protocols, some signal degradation was still observed on longer sequence acquisitions. This was most commonly seen in the highest b value subcomponents of the ADC maps, and likely explains the observed range of ADC quantitations that at times reach supra-physiologic values. Future studies in larger animal models, or as part of human trials, might achieve larger or more significant differences in the measurements evaluated by employing protocol design to mitigate these effects. In addition, we only evaluated a single time point, immediately post-therapy, to optimize our correlation with histopathologic results. Further study of T2, gagCEST and ADC at additional post-treatment time points in

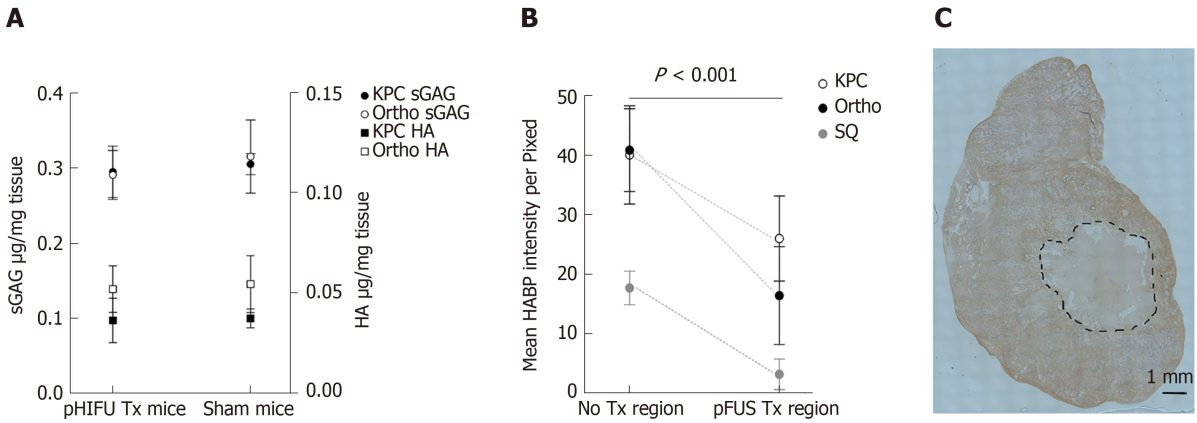

Figure 3 Histochemical and biochemical parameter changes due to pulsed focused ultrasound treatments. A: Hyaluronic acid (HA) and sulfated glycosaminoglycan concentrations in treated and sham treated KPC and orthotopic mice; B: HA intensities in treated and non-treated regions of the tumor in KPC, orthotopic, and subcutaneous models; C: Representative histological image of HA binding protein stained section for a KPC mouse. The treated region is outline by a dashed line. KPC: Genetic mouse model; Ortho: Orthotopic; HA: Hyaluronic acid.

survival studies would help to determine the optimal interval for post-treatment imaging and further elucidate the prognostic value of our results.

Conclusions

The use of a non-invasive technique such as MRI could be a useful tool for the evaluation of therapies used to treat PDA. It is likely that several different sequences would be needed to provide information on the microenvironment of the tumor. From this study, T2 relaxation, gagCEST, and ADC values have been identified to be part of the portfolio of scans which may provide reliable quantitation of pFUS treatment effects for patients with PDA.

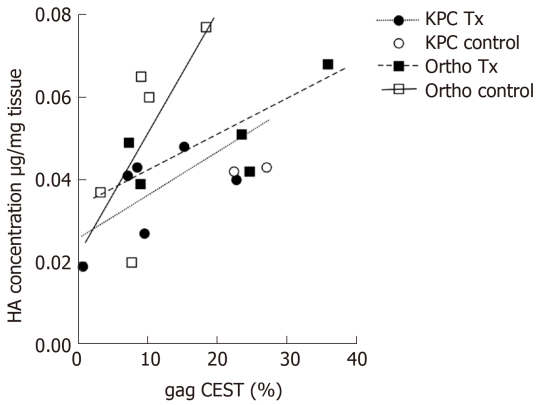

Figure 4 Total hyaluronic acid concentration compared to glycosaminoglycan chemical exchange saturation transfer for treated and sham treated (control) KPC and orthotopic mice. Regression lines for each animal model and condition demonstrate strong positive correlation between the hyaluronic acid concentrations as determined by the biochemical assay and glycosaminoglycan chemical exchange saturation transfer measurements. HA: Hyaluronic acid; CEST: Chemical exchange saturation transfer.

ARTICLE HIGHLIGHTS

Research background

The robust fibroinflammatory stroma characteristic of pancreatic ductal adenocarcinoma (PDA) impedes effective drug delivery. Pulsed focused ultrasound (pFUS) can disrupt this stroma and has improved survival in an early clinical trial. Non-invasive methods to characterize pFUS treatment effects are desirable for advancement of this promising treatment modality in larger clinical trials.

Research motivation

In this study, our objective was to identify non-invasive MRI methods that can be used to assess pFUS treatment effects for PDA, based on data derived from three murine models of PDA, including a genetic model. These methods have translational relevance to future, larger clinical trials that might help to advance pFUS therapy as a valuable supplement to traditional treatment modalities for patients with PDA.

Research objectives

Our primary objective was to identify promising, non-invasive pre-clinical imaging methods to characterize acute pFUS treatment effects for *in vivo* models of PDA. Robust pre-clinical data such as this builds critical foundation to facilitate efficient clinical trials. Knowledge of reliable methods to characterize the acute phase of treatment also helps to inform selection of methods to characterize long-term treatment follow up assessments in future studies.

Research methods

We utilized quantitative MRI methods at 14 tesla in three mouse models of PDA (subcutaneous, orthotopic and transgenic - *KrasLSL-G12D/+*, *Trp53LSL-R172H/+*, *Cre* or "KPC") to assess immediate tumor response to pFUS treatment (VIFU 2000 Alpinion Medical Systems; 475 W peak electric power, 1 millisecond pulse duration, 1 Hz, duty cycle 0.1%) *vs* sham therapy, and correlated our results with histochemical data. These pFUS treatment parameters were previously shown to enhance tumor permeability to chemotherapeutics. T1 and T2 relaxation maps, high (126, 180, 234, 340, 549) *vs* low (7, 47, 81) *b*-value apparent diffusion coefficient (ADC) maps, magnetization transfer ratio (MTR) maps, and chemical exchange saturation transfer (CEST) maps for the amide proton spectrum (3.5 parts per million or "ppm") and the glycosaminoglycan spectrum (0.5-1.5 ppm) were generated and analyzed pre-treatment, and immediately post-treatment, using ImageJ. Animals were sacrificed immediately following post-treatment imaging. The whole-tumor was selected as the region of interest for data analysis and subsequent statistical analysis. *T*-tests and Pearson correlation were used for statistical inference.

Research results

Mean high-*b* value ADC measurements increased significantly with pFUS treatment for all models. Mean glycosaminoglycan CEST and T2 measurements decreased significantly post-treatment for the KPC group. Mean MTR and amide CEST values increased significantly for the KPC group. Hyaluronic acid focal intensities in the treated regions were significantly lower following pFUS treatment for all animal models. The MRI changes observed acutely following pFUS therapy likely reflect: (1) Sequelae of variable degrees of microcapillary hemorrhage (T1, MTR and amide CEST); (2) Lower PDA glycosaminoglycan content and associated water content (glycosaminoglycan CEST, T2 and hyaluronic acid focal intensity); and (3) Improved tumor diffusivity (ADC) post pFUS treatment.

Research conclusions

T2, glycosaminoglycan CEST, and ADC maps proved to be reliable means of quantifying pFUS treatment effects in murine models of PDA, and may provide reliable, non-invasive quantitation of acute pFUS treatment effects for patients with PDA in future clinical trials.

Research perspectives

We have identified specific MRI methods as reliable non-invasive means of quantitating acute pFUS treatment effects for murine models of PDA. Future studies of long-term post-treatment disease burden may also benefit from employing the methods we describe. Clinical trials of pFUS therapy for PDA will be more easily accomplished if similar non-invasive methods of tracking immediate treatment endpoints can replace potentially morbid biopsies of this highly sensitive anatomic area. pFUS therapy may also be more efficacious for certain subpopulations of patients with PDA, and the methods we describe may help to non-invasively select enriched patient populations that will derive the greatest benefit from pFUS treatments in future studies.

ACKNOWLEDGEMENTS

We would like to thank Daniel S Hippe, biostatistician at the University of Washington, for reviewing the content of our manuscript to confirm appropriateness of biostatistical methods for study design.

REFERENCES

1 **Siegel RL**, Miller KD, Jemal A. Cancer statistics, 2019. *CA Cancer J Clin* 2019; **69**: 7-34 [PMID: 30620402 DOI: 10.3322/caac.21551]
2 **DuFort CC**, DelGiorno KE, Carlson MA, Osgood RJ, Zhao C, Huang Z, Thompson CB, Connor RJ, Thanos CD, Scott Brockenbrough J, Provenzano PP, Frost GI, Michael Shepard H, Hingorani SR. Interstitial Pressure in Pancreatic Ductal Adenocarcinoma Is Dominated by a Gel-Fluid Phase. *Biophys J* 2016; **110**: 2106-2119 [PMID: 27166818 DOI: 10.1016/j.bpj.2016.03.040]
3 **Jacobetz MA**, Chan DS, Neesse A, Bapiro TE, Cook N, Frese KK, Feig C, Nakagawa T, Caldwell ME, Zecchini HI, Lolkema MP, Jiang P, Kultti A, Thompson CB, Maneval DC, Jodrell DI, Frost GI, Shepard HM, Skepper JN, Tuveson DA. Hyaluronan impairs vascular function and drug delivery in a mouse model of pancreatic cancer. *Gut* 2013; **62**: 112-120 [PMID: 22466618 DOI: 10.1136/gutjnl-2012-302529]
4 **Li T**, Wang YN, Khokhlova TD, D'Andrea S, Starr F, Chen H, McCune JS, Risler LJ, Mashadi-Hossein A, Hingorani SR, Chang A, Hwang JH. Pulsed High-Intensity Focused Ultrasound Enhances Delivery of Doxorubicin in a Preclinical Model of Pancreatic Cancer. *Cancer Res* 2015; **75**: 3738-3746 [PMID: 26216548 DOI: 10.1158/0008-5472.CAN-15-0296]
5 **Yu MH**, Lee JY, Kim HR, Kim BR, Park EJ, Kim HS, Han JK, Choi BI. Therapeutic Effects of Microbubbles Added to Combined High-Intensity Focused Ultrasound and Chemotherapy in a Pancreatic Cancer Xenograft Model. *Korean J Radiol* 2016; **17**: 779-788 [PMID: 27587968 DOI: 10.3348/kjr.2016.17.5.779]
6 **Dimcevski G**, Kotopoulis S, Bjånes T, Hoem D, Schjøtt J, Gjertsen BT, Biermann M, Molven A, Sorbye H, McCormack E, Postema M, Gilja OH. A human clinical trial using ultrasound and microbubbles to enhance gemcitabine treatment of inoperable pancreatic cancer. *J Control Release* 2016; **243**: 172-181 [PMID: 27744037 DOI: 10.1016/j.jconrel.2016.10.007]
7 **Farr N**, Wang YN, D'Andrea S, Gravelle KM, Hwang JH, Lee D. Noninvasive characterization of pancreatic tumor mouse models using magnetic resonance imaging. *Cancer Med* 2017; **6**: 1082-1090 [PMID: 28390098 DOI: 10.1002/cam4.1062]
8 **Hingorani SR**, Wang L, Multani AS, Combs C, Deramaudt TB, Hruban RH, Rustgi AK, Chang S, Tuveson DA. Trp53R172H and KrasG12D cooperate to promote chromosomal instability and widely metastatic pancreatic ductal adenocarcinoma in mice. *Cancer Cell* 2005; **7**: 469-483 [PMID: 15894267 DOI: 10.1016/j.ccr.2005.04.023]
9 **Tseng WW**, Winer D, Kenkel JA, Choi O, Shain AH, Pollack JR, French R, Lowy AM, Engleman EG. Development of an orthotopic model of invasive pancreatic cancer in an immunocompetent murine host. *Clin Cancer Res* 2010; **16**: 3684-3695 [PMID: 20534740 DOI: 10.1158/1078-0432.CCR-09-2384]
10 **Maloney E**, DuFort CC, Provenzano PP, Farr N, Carlson MA, Vohra R, Park J, Hingorani SR, Lee D. Non-Invasive Monitoring of Stromal Biophysics with Targeted Depletion of Hyaluronan in Pancreatic Ductal Adenocarcinoma. *Cancers (Basel)* 2019; **11** [PMID: 31167451 DOI: 10.3390/cancers11060772]
11 **Desmond KL**, Moosvi F, Stanisz GJ. Mapping of amide, amine, and aliphatic peaks in the CEST spectra of murine xenografts at 7 T. *Magn Reson Med* 2014; **71**: 1841-1853 [PMID: 23801344 DOI: 10.1002/mrm.24822]
12 **Jin T**, Wang P, Zong X, Kim SG. MR imaging of the amide-proton transfer effect and the pH-insensitive nuclear overhauser effect at 9.4 T. *Magn Reson Med* 2013; **69**: 760-770 [PMID: 22577042 DOI: 10.1002/mrm.24315]
13 **Kim M**, Gillen J, Landman BA, Zhou J, van Zijl PC. Water saturation shift referencing (WASSR) for chemical exchange saturation transfer (CEST) experiments. *Magn Reson Med* 2009; **61**: 1441-1450 [PMID: 19358232 DOI: 10.1002/mrm.21873]
14 **Schneider CA**, Rasband WS, Eliceiri KW. NIH Image to ImageJ: 25 years of image analysis. *Nat Methods* 2012; **9**: 671-675 [PMID: 22930834 DOI: 10.1038/nmeth.2089]
15 **Kim S**, Decarlo L, Cho GY, Jensen JH, Sodickson DK, Moy L, Formenti S, Schneider RJ, Goldberg JD, Sigmund EE. Interstitial fluid pressure correlates with intravoxel incoherent motion imaging metrics in a mouse mammary carcinoma model. *NMR Biomed* 2012; **25**: 787-794 [PMID: 22072561 DOI: 10.1002/nbm.1793]
16 **Schmitt B**, Zbýn S, Stelzeneder D, Jellus V, Paul D, Lauer L, Bachert P, Trattnig S. Cartilage quality assessment by using glycosaminoglycan chemical exchange saturation transfer and (23)Na MR imaging at 7 T. *Radiology* 2011; **260**: 257-264 [PMID: 21460030 DOI: 10.1148/radiol.11101841]

17 **Haris M**, Singh A, Reddy S, Bagga P, Kneeland JB, Tjoumakaris FP, Hariharan H, Marincola FM, Reddy R. Characterization of viscosupplementation formulations using chemical exchange saturation transfer (ViscoCEST). *J Transl Med* 2016; **14**: 92 [PMID: 27071650 DOI: 10.1186/s12967-016-0850-8]

18 **Li T**, Chen H, Khokhlova T, Wang YN, Kreider W, He X, Hwang JH. Passive cavitation detection during pulsed HIFU exposures of ex vivo tissues and in vivo mouse pancreatic tumors. *Ultrasound Med Biol* 2014; **40**: 1523-1534 [PMID: 24613635 DOI: 10.1016/j.ultrasmedbio.2014.01.007]

19 **Chevillet JR**, Khokhlova TD, Giraldez MD, Schade GR, Starr F, Wang YN, Gallichotte EN, Wang K, Hwang JH, Tewari M. Release of Cell-free MicroRNA Tumor Biomarkers into the Blood Circulation with Pulsed Focused Ultrasound: A Noninvasive, Anatomically Localized, Molecular Liquid Biopsy. *Radiology* 2017; **283**: 158-167 [PMID: 27802108 DOI: 10.1148/radiol.2016160024]

20 **Ma X**, Bai Y, Lin Y, Hong X, Liu T, Ma L, Haacke EM, Zhou J, Wang J, Wang M. Amide proton transfer magnetic resonance imaging in detecting intracranial hemorrhage at different stages: a comparative study with susceptibility weighted imaging. *Sci Rep* 2017; **7**: 45696 [PMID: 28374764 DOI: 10.1038/srep45696]

21 **Battini S**, Faitot F, Imperiale A, Cicek AE, Heimburger C, Averous G, Bachellier P, Namer IJ. Metabolomics approaches in pancreatic adenocarcinoma: tumor metabolism profiling predicts clinical outcome of patients. *BMC Med* 2017; **15**: 56 [PMID: 28298227 DOI: 10.1186/s12916-017-0810-z]

22 **Vohra R**, Park J, Wang YN, Gravelle K, Whang S, Hwang JH, Lee D. Evaluation of pancreatic tumor development in KPC mice using multi-parametric MRI. *Cancer Imaging* 2018; **18**: 41 [PMID: 30409175 DOI: 10.1186/s40644-018-0172-6]

23 **Theocharis AD**, Tsara ME, Papageorgacopoulou N, Karavias DD, Theocharis DA. Pancreatic carcinoma is characterized by elevated content of hyaluronan and chondroitin sulfate with altered disaccharide composition. *Biochim Biophys Acta* 2000; **1502**: 201-206 [PMID: 11040445 DOI: 10.1016/s0925-4439(00)00051-x]

24 **Lee SS**, Byun JH, Park BJ, Park SH, Kim N, Park B, Kim JK, Lee MG. Quantitative analysis of diffusion-weighted magnetic resonance imaging of the pancreas: usefulness in characterizing solid pancreatic masses. *J Magn Reson Imaging* 2008; **28**: 928-936 [PMID: 18821618 DOI: 10.1002/jmri.21508]

25 **Gebauer F**, Kemper M, Sauter G, Prehm P, Schumacher U. Is hyaluronan deposition in the stroma of pancreatic ductal adenocarcinoma of prognostic significance? *PLoS One* 2017; **12**: e0178703 [PMID: 28582436 DOI: 10.1371/journal.pone.0178703]

Published By Baishideng Publishing Group Inc
7041 Koll Center Parkway, Suite 160, Pleasanton, CA 94566, USA
Telephone: +1-925-3991568
E-mail: bpgoffice@wjgnet.com
Help Desk:http://www.f6publishing.com/helpdesk
http://www.wjgnet.com